EXTENSION OF A PROGRESSIVE FAILURE, ENERGY DISSIPATION, COMPOSITE TAILORING CONCEPT TO A HEALING CONFIGURATION

by

SHAILESH JAYANT DIVEY

Presented to the Faculty of the Graduate School of

The University of Texas at Arlington in Partial Fulfillment

of the Requirements

for the Degree of

MASTER OF SCIENCE IN MATERIALS SCIENCE AND ENGINEERING

THE UNIVERSITY OF TEXAS AT ARLINGTON

August 2011

Copyright © by Shailesh Jayant Divey 2011

All Rights Reserved

ACKNOWLEDGEMENTS

I would like to express my gratitude to my Academic Advisor, Dr. D. Stefan Dancila for his support, guidance and mentoring. This work would not have been possible without his contribution.

I am grateful to Dr. Xinyuan Tan and Dr. Jennifer Goss for their guidance during the initial stages of the study and research. I am immensely grateful to Dr Robert Haynes for his constant guidance, which helped me bring my research to fruition. I am also indebted to all my professors at The University of Texas at Arlington for a wonderful learning experience. I would also like to acknowledge the interaction with my other colleagues at the University, Urmi Khode Julia Cline, Sthanu Mahadev, Daniel Mockler, Michael Tadros and Yassine Benjellou.

Finally, and most importantly, I would like to thank my parents, Mr. Jayant D. Divey and Mrs. Veena J. Divey for their unconditional love, support and sacrifice. Their prolific achievements and endless ambitions in their professional and personal lives set extremely high standards for me to try and emulate. Their encouragement drives me towards success. I also thank my sister, Ms. Sharvari J. Divey for supporting and encouraging me and at the same time challenging me with intellectual discussions.

July 14, 2011

ABSTRACT

EXTENSION OF A PROGRESSIVE FAILURE, ENERGY DISSIPATION, COMPOSITE TAILORING CONCEPT TO A HEALING CONFIGURATION

Shailesh Jayant Divey, M.S.

The University of Texas at Arlington, 2011

Supervising Professor: D. Stefan Dancila

A composite failure tailoring concept that results in a yield type response under tension has been proposed, modeled, and experimentally verified in prior research. The concept capitalizes upon a sequential, progressive failure of a set of redundant load paths of tailored strength and length. It has been shown in prior publications that the concept is functional and by comparison with experimental results that the analytical models of response developed are accurate. The limits of performance of the proposed tailoring concept have recently been investigated via a parametric study using one of the response models developed and significant improvements have been shown over the performance demonstrated in the earlier work.

One of the limitations of the original concept consists in its single-use characteristic, due to the irreversibility of the fracture processes involved. In this study, the failure tailoring concept is extended to a configuration that has the capacity to reconstitute itself after the loading event. This is accomplished by the use of a set of magnets in the primary load path while continuing to use high performance fiber composites for the secondary load path and the connectors. The ability of the primary load path magnets to reattach to each other, thereby reconstituting the primary load path, provides an overall structural healing capability while

preserving the energy dissipation characteristic of the original concept implementation. Analytical modeling is provided. This new, extended tailoring concept implementation provides a bridge towards smaller, meso- (fiber level) and nano-scale (molecular) level implementations. However, it must be noted that the model is only of importance for illustrating the concept of healing. The healing features render the new concept of interest for applications such as space tethers.

TABLE OF CONTENTS

LIST OF ILLUSTRATIONS

LIST OF TABLES

CHAPTER 1

INTRODUCTION

"As a general principle natural selection is continually trying to economize every part of the organization."

- Charles Darwin

Charles Darwin proposed that revolutionary scientific theory of natural selection that revealed the pattern of evolution of life. This theory endorses the rule of 'survival of the fittest', which is one of the truest and the most successful optimization algorithms in nature. Damage prevention has been the basis of developing engineering materials with desired properties for many centuries i.e. materials are designed to maximize their service life as a function of load and time. Biological materials have remarkably efficient mechanisms of resisting loads, fracture, buckling and survive damage. However, the most exceptional functional ability of biological materials is their ability to self-repair.

1.1 Motivation

The ability of the materials in nature to self-heal assumes great importance from the economic standpoint in case of structural materials. The concept of damage management realizes and acknowledges the high probability of the occurrence of damage in service structures but is not overwhelmed by it as long as an autonomous process of repair counteracts it. Damage management characterizes natural materials like skin tissue and bone structures that self-repair and nearly restore the original functionality of the material. If the concept of damage management were to be successfully incorporated into artificial structural materials such as composites, concrete and even steel, it could result in simplification and reduction in costs for examining and evaluating structures. Understanding the functional characteristics of

natural systems in order to produce systems that work feasibly and economically with engineering structures is the major challenge for developing self-healing materials.

1.2 Background

Strength of a material relates to its ability to sustain a high load before it eventually fails. Toughness of a material relates to its ability to absorb energy before failure. Achieving high levels of both strength and toughness can improve the performance of the material. A class of materials that has established itself as having the potential for high strength is composites. The ability to tailor the structural properties of composite materials has increased their worldwide demand. One such tailoring mechanism has been demonstrated to improve toughness.

However, the ability to experience damage caused by loading and afterwards initiate healing is a revolutionary concept in material design. A relatively large volume of research conducted on self-healing materials involved polymer based systems, which are an important type of composite materials. Self-healing mechanisms in concrete, ceramics, asphalt too have also been explored. The development of self-healing materials is still in early stages and the identification of properties that allow a material to self-heal is very crucial.

Table 1.1 provides a comparison between the properties of ideal and minimal self-healing materials.

Table 1.1. Properties of “ideal” and “minimal” self-healing materials [1]

Ideal Self-Healing Material	**Minimal Self-Healing Material**
Can heal damage many times	Can heal damage only once
Can heal damage completely	Can heal damage partially
Can heal defects of any size	Can heal small defects only
Performs healing autonomously	Require external assistance to heal
Equal/Superior properties to current materials	Inferior properties to current materials
Cheaper than current materials	Extremely expensive

The materials being developed currently are closer to “minimal” self-healing materials because developing a material that heals autonomously i.e. without any external assistance whatsoever is a bigger challenge. The feasibility of this method is still unresolved.

1.3 Space Tether Problem

Space tethers are long cables made of high-strength fibers or conducting wires and are used to couple spacecraft to other spacecraft or masses such as a spent booster rocket, space station or an asteroid [2]. The applications envisioned for space tethers are momentum-exchange, propellant-less propulsion and formation flying. Spectra, used to make fishing lines, has been used previously to manufacture the tethers. In the near future, tethers maybe made out of spider silk or carbon nanotube composite fibers. An example of a tether is the Hoytether [3], developed by Robert P. Hoyt, which utilizes tubular interwoven lattice much like fishing net to limit damage due to micrometeoroids and orbital debris to one strand.

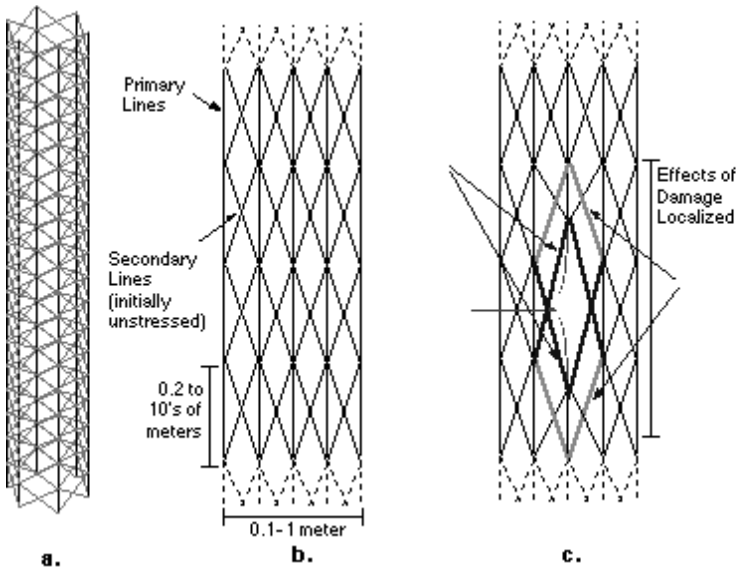

Figure 1.1 The Hoytether concept. a) tubular section of hoytether. b) intact tether. c) damaged tether.

1.3.1 Strength Criteria for Tethers

Tethers are long structures with a potential for structural failure at a single point. Two solutions to improve toughness are through sequential failure with redundant load paths [4] or multi-strand tethers with redundant interlinking that have the ability to withstand multiple impacts from space debris [3]. These solutions simply increase the service life of the tether. The failure processes involved are irreversible. Autonomous-healing materials make an effort to address this irreversibility.

CHAPTER 2

LITERATURE SURVEY

Due to the manifold advantages of polymer matrix composites like high specific strength and stiffness and their anisotropic nature, which allows additional degrees of freedom for design and advantages in terms of manufacturability, they are rapidly replacing metal parts in the aerospace industry [5]. However, their susceptibility to matrix cracking on impact and their brittle nature has led to research towards improving damage prediction and structural repair. Polymeric materials that mimic the self-healing functionality of biological systems have been developed to increase the service life of engineering materials. Some of these developments are discussed below.

2.1 Design #1: Microencapsulation

Microencapsulation accomplishes self-healing by embedding a microencapsulated healing agent in a structural composite matrix that contains a catalyst, which is capable of polymerizing the liquid healing agent. It is essential that the healing agent remains stable inside the microcapsules without reacting, until it is released into the crack. Cracks occur when a material is damaged, and it ruptures the microcapsules, thereby releasing the liquid healing agent into the crack plane through capillary action. Contact with the catalyst triggers polymerization that closes the crack faces. The liquid healing agent used is a monomer, dicyclopentadiene (DCPD), which is encapsulated in a urea-formaldehyde microcapsule and the catalyst used is Bis(tricyclohexylphosphine)benzylidine ruthenium (IV) dichloride, also otherwiseknown as Grubbs' catalyst [6-10]. The crack healing occurs by a ring-opening metathesis polymerization (ROMP). The healing mechanism is shown in Figure 2.1.

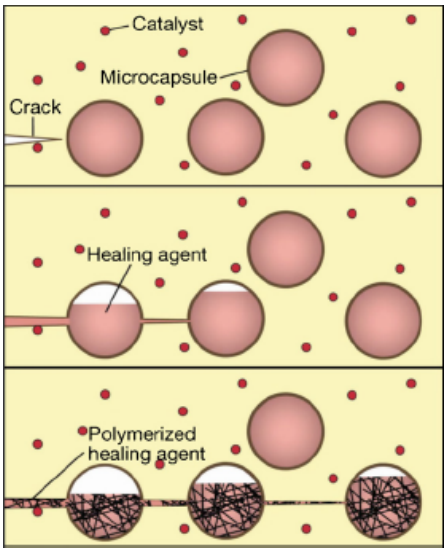

Figure 2.1 Concept of microencapsulation. [10]

In addition to acting as healing agent storage units, the microcapsules also significantly improve the fracture toughness of the polymer matrix by limiting crack growth and propagation via crack pinning mechanism. Mechanical tests performed on such specimens indicate that a material allowed to self-heal at room temperature achieves healing effectiveness of about 85±5% [6]. However, this system has its drawbacks too, such as the depletion of healing reagents and the high cost of Grubbs' catalyst, thereby limiting the commercial scale manufacturing and applications of the self-healing material. Incorporating the catalyst and the microcapsules reduces the virgin inter-laminar toughness. This is believed to happen due to an increase in the inter-laminar thickness from the size and concentration of microcapsules along with difficulty in dispersion of catalyst. Agglomeration of catalyst also contributes to unstable crack propagation. However, an improvement of matrix resin toughness by about 127% proves that it is possible to achieve a tougher structural composite if the manufacturing and processing techniques can be refined and optimized. An even dispersion of even smaller microcapsules would also aid in the repair of small-scale damages and not simply delaminations on a large scale [5].

2.2 Design #2: Microvascular Network

The concept of microvascular network is similar to that of microencapsulation in that the matrix material, healing agent and the catalyst used are the same. However, instead of the healing agent being embedded into spheres, it is dispersed in a three-dimensional network of micro-channels. The healing process here is similar to that in microencapsulation as the healing agent is released from the micro-channels when damage occurs and enters the crack by capillary action. Here, an epoxy coating is deposited on a ductile substrate containing the 3-D micro-channel network. This concept mimics the human skin in its self-healing functionality, specifically the epidermal layer that rebuilds the surface of the skin on injury. So as to not compromise the structural integrity of the sample, it is desirable to have networks with maximum channel spacing and minimum channel diameter. Figure 2.2 depicts the concept of microvascular networks.

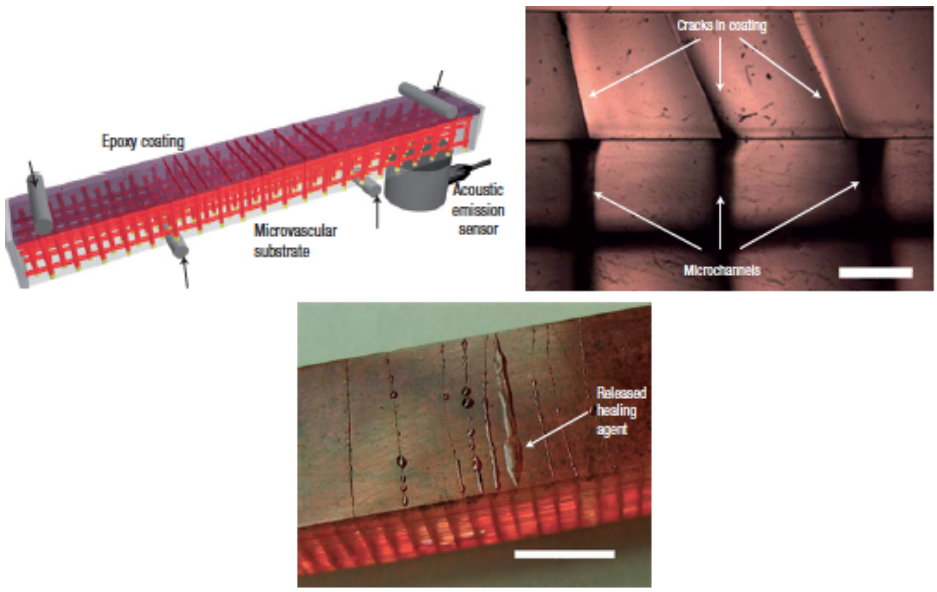

Figure 2.2 Concept of microvascular network healing showing, clockwise from left to right, schematic diagram of the self-healing structure, cross-sectional image of cracks propagating towards the micro-channel opening, and optical image of self-healing structure after cracks are formed. [12]

The micro-channels are manufactured by a robotic direct-write assembly [11], which is a technique capable of producing three-dimensional periodic structures comprised of cylindrical

rods. They are then filled from the side of the composite sample via the horizontal channels. The channels are made out of EnviroTex Lite epoxy, which is less brittle as compared to the epoxy matrix.

The efficiency of the process is determined by the ability of the coating to recover its fracture toughness. The advantage of this method over microencapsulation is the multi-use feature of the healing agent until it is completely depleted. The healing effectiveness of the material gets degraded when there is not more supply of the catalyst even though there still is continuous supply of the monomer.

However, this method has its drawbacks due the high costs involved due to the network manufacturing process by using the robotic assembly. Another drawback is the depletion of the self-healing agent after multiple healing events. This drawback needs to be addressed in order to make the material truly autonomous-healing.

2.3 Design #3: Hollow Tubes

Repeated healing is possible if there is a continuous supply of liquid healing agent available. Dry et al. [13-14] approached this problem with hollow tubes or fibers as a solution, but with limited success. Their attempts were limited by the large diameter of the capillaries and the choice of healing agents used. A process to optimize the production of hollow glass fibers has been developed by Bond and co-workers [15-18]. Their process uses the glass fibers filled with the liquid healing agents or dyes for detecting damage as well as self-healing, a dual functionality. When static loading damages composite panels containing the hollow fibers, the damage site is observed to recover about 87% of its measured baseline flexural strength [16]. A similar approach by Pang et al. [18] was successful in recovering about 97% of the original, undamaged flexural strength. The major advantage of this method is that it permits flexibility in design such that it allows healing plies to be placed at different locations within the laminate.

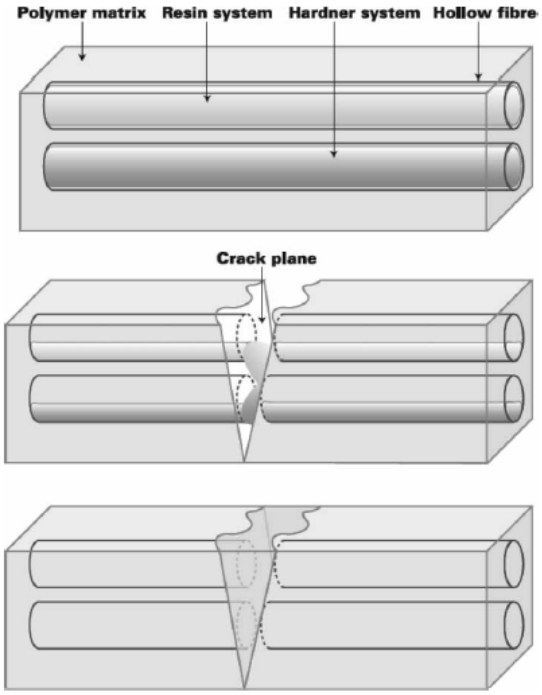

Figure 2.3 Concept of self-healing using hollow tubes or fibers [5, 15]

2.4 Design #4: Shape Memory Polymer Composites

An integrated system of shape memory polymer (SMP) composites and structural health monitoring has been explored to repair structural damage caused by impact like debris. This system should help in increasing the service life of aerospace vehicles and aero-structures while also enhancing crew and payload protection. This can be accomplished by the integration of two emerging technologies- structural health monitoring and intelligent controls. Composite systems composed of healable polymer matrix undergo healing on subsequent damage and recover about 90% of original mechanical performance. Heating the composite above its activation temperature does this, whereupon it reverts back to its shape upon becoming soft and pliable.

The composite system contains an outlying grid of piezoelectric sensors, which generate a charge under mechanical loading. The healing cycle is initiated by the intelligent control system, which detects anomalies, and signals integrated heating elements to heat the

damaged area. This causes the damage site to return to near-manufactured state due to the shape memory effect and matrix healing, thereby aiding in the recovery of a significant amount of mechanical performance. This technique has been developed and marketed by the Cornerstone Research Group (Dayton, OH 45440) for commercial applications.

Besides shape memory polymer composites comprised of carbon fibers, conducting metals and certain metal alloys can be used to induce healing through electrical resistive heating [19]. When shape memory alloy (SMA) wires are coupled with wax encapsulated healing agent embedded in an epoxy matrix, they have a dual effect. First, contraction of SMA wire upon heating exerts a force that is sufficient enough to close a crack by a substantial amount, thereby reducing the amount of healing agent required to heal the crack. Second, the heated SMA wires allow greater curing and better adhesion of healing agent to achieve higher healing efficiency [20]. The increase in healing effectiveness observed ranges from 77% to 98% with the wires, while the healing effectiveness without wires is observed to be 49%. Therefore, the desired result of greater mechanical properties of the cured healing agent is achieved.

2.5 Design #5: Supramolecular Networks

Reversible bonds, such as hydrogen bonds, characterize supramolecular interactions and researchers are exploring this inherent property extensively [21-24]. However, an unfortunate trade-off for this property is low mechanical strength. Work has been done to avoid this drawback by increasing the number of interactions within the material [25]. Healing in a material is therefore enabled by the reversibility of these multiple interactions.

2.5.1. Hydrogen Bonding

A supramolecular healable rubber recently studied by Cordier et al. is formed by hydrogen bonding [26]. The resulting material however requires mechanical stimulus to undergo healing, due to the site-specific property of hydrogen bonding. Amido imidazolidones and urea were the hydrogen-bond forming groups used in the material and they were mixed in a way

such that they maintain the elastomeric properties of the material without forming any crystalline regions.

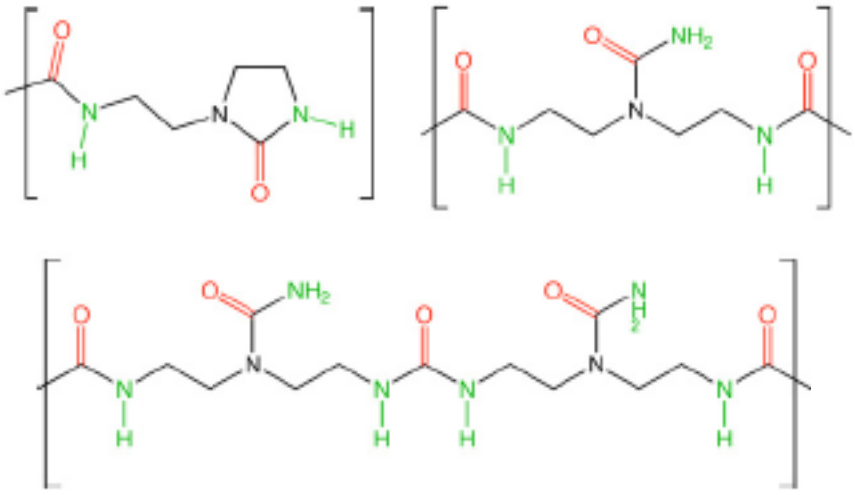

Figure 2.4 Supramolecular networks with hydrogen bonding - fatty diacid mixture (upper left) reacts with urea (upper right) to produce a mixture of oligomers (where, red denotes hydrogen bond acceptors, and green denotes hydrogen bond donors) [26]

2.5.2. Metal-Ligand Coordination

Another supramolecular interaction that has been explored for its use in self-healing materials is metal-ligand coordination. The inclusion of a metal-ligand complex in a polymer system was first reported by Kersey et al. [27]. A polymer network with covalent bonding containing pyridine pendant groups was created, which formed a metal-ligand coordination complex with a bifunctional Pd(II) or Pt(II) compound. Stress bearing groups composed of a pyridine functionalized methacrylate cross-linked network were incorporated into a hybrid polymer gel. The mechanical properties of the network containing metal complexes were measured and found to be greater than the properties of the polymer network itself. Although this system requires mechanical stimulation, it is an interesting step towards self-healing.

2.6 Mechanical Testing and Quantification of Healing Effectiveness

Healing effectiveness is defined in the terms of recovery of fracture toughness [10]. Wool and O'Conner [28] defined crack healing effectiveness (η) as,

$$\eta = (K_{IC}^{healed} / K_{IC}^{virgin}) * 100\% \quad (2.1)$$

where, K_{IC}^{healed} is the mode I fracture toughness of a healed specimen, and K_{IC}^{virgin} is the mode I fracture toughness of the virgin, undamaged specimen.

Based on the ability to recover fracture energy, an alternative definition has been proposed as follows,

$$\eta_G = (G_{IC}^{healed} / G_{IC}^{virgin}) * 100\% \quad (2.2)$$

where, G_{IC}^{healed} is the rate of critical release of energy on testing a healed fracture specimen, and G_{IC}^{healed} is the rate of critical release of energy on testing a virgin specimen.

The healing effectiveness in the above equations are related as

$$\eta = \sqrt{\eta_G} \quad (2.3)$$

These definitions are applicable for mode I loading conditions, although the analysis is similar for mode II, III and mixed mode fractures. It is interesting to know that since a fracture test requires the presence of a precrack to measure the fracture toughness, healing effectiveness greater than 100% can be obtained.

Rule et al. [9] defined healing efficiency in terms of internal work (or strain energy) to account for non-linear elastic behavior observed in the presence of dissolved wax when the healing agent is encapsulated in wax microcapsules.

$$\eta' = U_{healed} / [b_n(W - a_{0_{healed}})] \Big/ U_{virgin} / [b_n(W - a_{0_{virgin}})] \quad (2.4)$$

where, U_{healed} and U_{virgin} represent the area under the load-displacement curve (strain-energy) during fracture testing, b_n gives the width of the crack surface, W is distance between the line of loading to the end of the specimen, and $a_{0healed}$ and $a_{0virgin}$ are the initial precrack lengths of the virgin and the healed specimen.

Sanada *et al*. [29] defined healing effectiveness in terms of tensile strength of the specimen, σ.

$$\eta_{tensile} = \sigma_C^{healed} \Big/ \sigma_C^{virgin} \tag{2.5}$$

In case of hollow fibers, healing effectiveness is defined in terms of residual flexural strength of the material.

$$\eta_{flexural} = (\sigma_{C_{flexural}}^{healed} - \sigma_{C_{flexural}}^{damaged}) \Big/ (\sigma_{C_{flexural}}^{virgin} - \sigma_{C_{flexural}}^{damaged}) \tag{2.6}$$

In addition to fracture testing, fatigue-healing efficiency [30, 31] is defined in terms of total number of failure cycles as follows,

$$\lambda = (N_{healed} - N_{control}) \Big/ (N_{control}) \tag{2.7}$$

Other approaches proposed towards determining healing efficiencies relate to change in stiffness [32], continuum healing mechanics [33-36] and residual stiffness and strength of microcracks [37].

Although a self-healing functionality is invaluable, it must not come at the expense of reduction in the virgin properties of the material, thereby compromising its structural integrity. While it has been reported that microcapsules induce toughening, linear decrease of in fracture toughness with respect to microcapsule content [38] implies that fracture toughness depends upon the specific nature of added constituents and matrix. The ability to heal microcracks would inhibit structural failure, thereby increasing the service life of structural materials. While the feasibility of large-scale crack and delamination repair have been demonstrated, self-healing at smaller viz. nanometer length scales would be more beneficial since the magnitude of damage at this scale is small. By repairing small-scale damage, critical large-scale damage like delamination can be delayed or even potentially prevented.

An alternative approach to self-healing would be one where a material toughness increases under the event of loading prior to fracture. Many self-healing systems currently being studied require external stimulus like mechanical, thermal, electromagnetic, photo or even ballistic. However, if a material could be tailored to combine progressive failure and subsequent

self-healing, it would have very high fracture toughness. An ideal autonomously healing material would repair instantly under a loading event and therefore be insusceptible to failure. There is subsequent dissipation of energy after every fracture and when a material heals, it typically does not recover 100% toughness. The fundamental problem, therefore, for creating a completely autonomously healing material, would be to track the dissipated energy.

An extension of a tailoring concept involving multiple load paths that result in sequential, progressive failure [4] has been proposed in this work as a possible alternative towards creating a completely autonomously healing material that is tailored to initiate healing without any external stimulus.

CHAPTER 3

CONCEPT DEVELOPMENT

Previous work on energy dissipating composite members that are characterized by progressive failure [4,39] investigated the feasibility of composite members with yield-type response under tensile loading and proposed a failure tailoring concept that investigated an axially-stiff and bend-wise flexible material consisting of high performance fibers and an elastomeric matrix. Current work explores the possibility of creating a structure (tether) that implements the original concept while also exhibiting the ability to self-heal.

3.1 Original Tailoring Concept – An Overview

An overview of the original failure-tailoring concept [4] has been provided in this section for convenience.

3.1.1. Dimensions of the Tailored Member

The functional unit of the tailored member described in the original failure-tailoring concept consists of a primary load path, a secondary load path, and a connector segment. The secondary load path is attached to the primary load path at regular intervals along the length of the member, known as the connector segment. The member consists of several identical links in series, and an example of a five-link member is shown in Figure 3.1. The primary segment, secondary segment and the connector are denoted as l_p, l_s, and l_c respectively, as shown in the detail of a link in Figure 3.2.

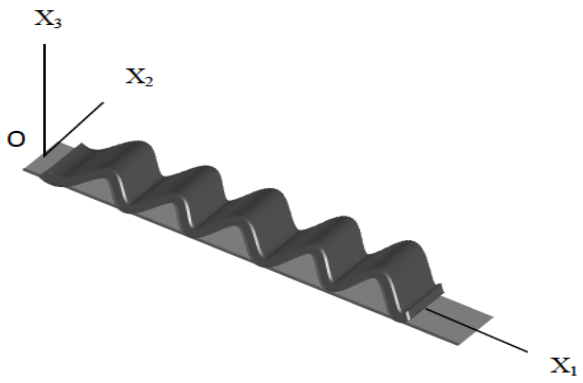

Figure 3.1 Isometric view of tailored member with five links [4]

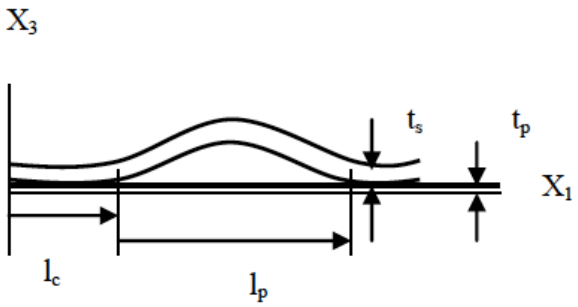

Figure 3.2 Single link [4]

The total length of the unbroken member is the sum of the lengths of the primary segment and the connectors, and is given as

$$L = (n+1)\, l_c + n\, l_p \tag{3.1}$$

The length of the primary and secondary segment depends upon the manufacturing process used to create the tailored member. The length of the connectors however, is governed by the shear modulus of the chosen material, and is designed such that failure will occur in the primary members before the connectors. The combined thickness of the composite member t, is given by,

$$t = t_p + t_s \tag{3.2}$$

where t_p and t_s are the thicknesses of primary and secondary segment respectively.

3.1.2. Behavior of the Tailored Member

The length of the secondary segment in each link must be greater than the length and thickness of the primary segment, such that the primary segment will load and fail prior to loading of the secondary segment within each link. When one primary segment fails, the load transfer between the links adjacent to the links containing the failure occurs through the connector between the two adjacent links. Upon tensile loading of the composite member, only the primary segments and the connectors carry the load. Because the primary segments are identical, theoretically they will fail simultaneously, however, in practice they fail sequentially in a stochastic process. Failure of a primary segment dissipates the strain energy that was stored in the system, but the resulting loading of the secondary segment prevents failure of the entire tether, thereby resulting in a beneficial loss (or dissipation) of energy in the system. The increased toughness of the system is a result of the redistribution of load among a network of redundant load path elements, which results in increased fracture surface area. This can be explained by suggesting that a brittle system (untailored member) dissipates very little energy on a single failure whereas on applying the tailoring concept, the energy-dissipation of the tailored member increases by a factor proportional to the number of links, thereby resulting in an increased toughness.

3.1.3 Response of the Tailored Member

The system behaves in a linearly elastic manner up to the point of failure of each segment. Figure 3.3 illustrates the typical yield-type response of the tailored member under quasi-static loading, along with the response of an equivalent un-tailored member which consists of the same material system, orientation, total length, and total cross-sectional area but has no detached secondary segment. The response of the untailored member resembles that of a brittle material while the tailored member exhibits a yield-type structural response.

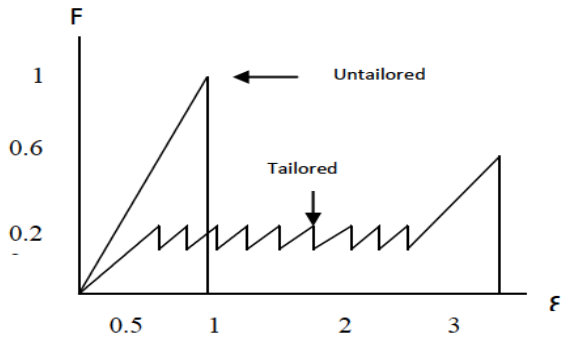

Figure 3.3 A typical yield-type response curve for a tailored member [4, 40]

This concept has been experimentally verified for members under quasi-static uniaxial loading and impulsive loadings. The results obtained have validated the failure tailoring concept and its increased energy dissipation capability too. Furthermore, a parametric study has investigated the toughening benefit achievable for the response and has found out that a tailored member can attain over 71 times the toughness of an untailored member [40].

3.2 Autonomously Healing Configuration - Analytical Model

This work describes a modification to the original tailoring concept that incorporates autonomous healing.

3.2.1 Description of the Model

First, high-power magnets are inserted in place of the primary segments. The failure of primary segments is equivalent to the separation. The high-power magnets are small yet powerful axially magnetized rare earth Neodymium magnets. Second, a high-performance fiber acts as the secondary load path. The entire magnet length can be considered as the connector segment, and the string runs along the length of the magnet. The connector segment transmits the load across the configuration.

The primary reason for choosing the magnets as the primary load path is their ability to exert considerably strong forces of attraction even when they are separated from each other. The magnetic attraction therefore acts as a restoring force, thereby enabling reconstitution.

Figure 3.4 shows an axially magnetized cylindrical magnet, with magnetic field lines running from the north pole to the south pole of the magnet.

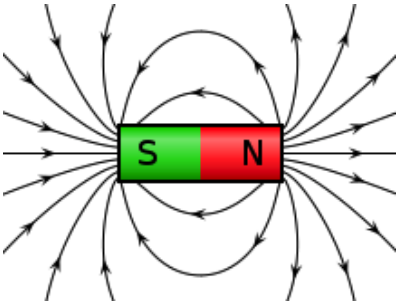

Figure 3.4 Magnetic field of an axially magnetized cylindrical magnet

The secondary segment in the original concept is an “axially stiff, bendwise flexible” [4] unidirectional composite, which has a significant amount of bending compliance, thereby allowing it to straighten upon the failure of the primary segment link. The use of a string (high-performance fiber) as the secondary load path in the healing configuration can be justified on similar lines. The important considerations taken into account while selecting the material for the string are its strength and stiffness. The strength of the string must be high enough such that it does not fail prior to the separation of any magnets. When a magnet separation occurs, a string length gets added to the length of the magnet-string configuration. This can be accomplished only if the bending compliance of the string is high enough such that it does not fail immediately after any magnet separation, thereby ensuring sequential, progressive failure.

A configuration consisting of three magnets in its unloaded and loaded state respectively has been illustrated in Figure 3.5.

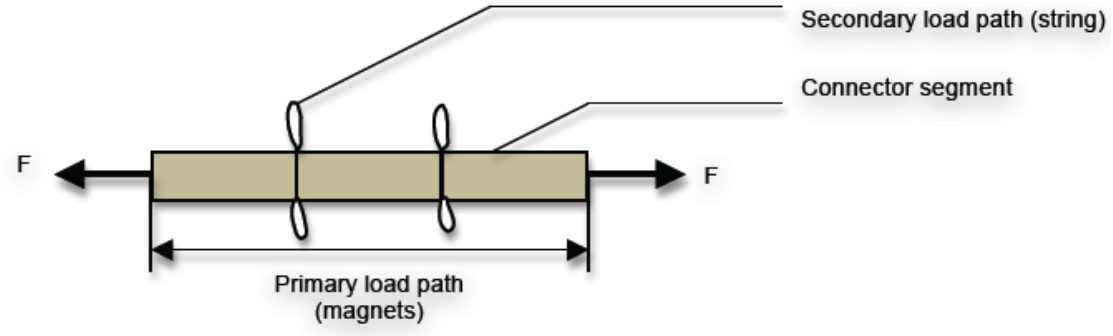

(a)

(b)

Figure 3.5 Magnet-string configurations (a) before loading (b) under loading

Figure 3.5 (b) shows the magnet configuration under loading beyond the point at which the primary segment has failed. However, in this case, the failure is replaced by magnet separation, although in this work magnet separation will continue to be referred to as failure. In the original tailoring concept proposed by Dancila *et al.* [4], when the tether is subjected to loading, the configuration is expected to experience sequential, progressive failure. Even after the magnets are separated, they still generate a weakened force of attraction towards the other magnets. Whereas in the original model, failure is irreversible, in this model, the magnets come back together after the applied load is removed, thereby constituting a configuration identical to the original configuration. This reconstituting feature characterizes the autonomous healing configuration. It follows that as long as the applied load is lower than the load required for the ultimate failure of the secondary load path, the configuration can be pulled apart and reconstituted an unlimited number of times without an evidence of previous history.

The methodology for determining whether the magnet configuration satisfies the condition of sequential, progressive failure involves calculating the magnetostatic interaction energy and attraction forces between magnets.

To model the healing configuration, it is essential to determine the force between two interacting magnets, which are shown in Figure 3.6. This is done by using the equations derived by Vokoun *et al* [41], which take into account the total magnetostatic interaction energy of the system.

$$F_z(\delta) = -8\pi K_d R^2 \int_0^\infty \frac{J_1^2(q)}{q} \sinh(q\tau_1)\sinh(q\tau_2)e^{-q\zeta}\, dq \qquad (3.3)$$

where, F_z is the attraction force between two magnets, $K_d=\mu_0 M^2/2$ is the magnetostatic energy constant. $\tau_i=l_i/(2R)$ is the aspect ratio of the magnets and $\zeta=Z/R$ is the reduced distance between the centers of the cylindrical magnets. $J_1(q)$ is a modified Bessel function of the first kind. Table 3.1, given below, describes the parameters used to determine the magnetic forces of attraction in Eq. 3.3.

Table 3.1 Parameters used to calculate force between magnets

Parameters	Description
μ_0	Permeability of vacuum (= 4π x 10^{-7} V.s/(A.m))
M	Magnetization of the magnet
R	Radius of the magnet
l	Length of the magnet
Z	Distance between the magnet centers

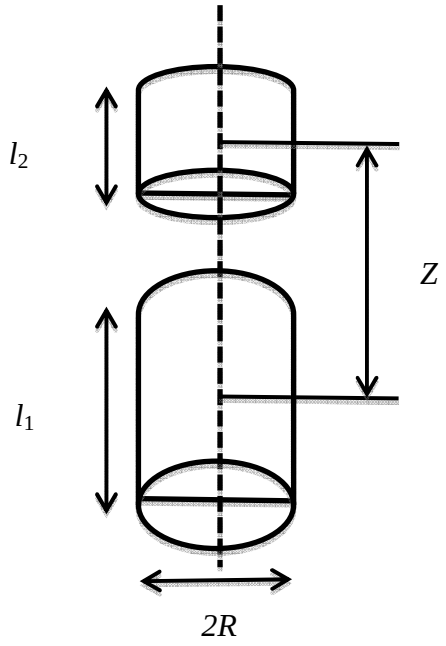

Figure 3.6 Interaction between two axially magnetized cylindrical permanent magnets

Given four or more magnets in series, by evaluating the attraction forces, it can be determined that the magnitude of force required for failure of the primary load path at an end is less than the magnitude required for the configuration to fail in any other manner. Subsequently, the primary load path of the configuration fails at either end, in a stochastic manner. For an n magnet configuration,

$$F_{i,n-i} > F_{i=1,n-1} \quad \text{, for } 2 \leq i \leq n\text{-}2 \tag{3.4}$$

$F_{i,n-i}$ denotes the force required to separate i magnets from n-i magnets in a linear sequence of n magnets. Similarly, $F_{1,n-1}$ denotes the force required to separate 1 magnet from n-1 magnets in a linear sequence of n magnets. Figure 3.7, as shown below, plots the variation in the force of separation (attraction) between magnets as a function of displacement between the magnets. Table 3.2 that follows the figure shows the values of the contact force between the magnets.

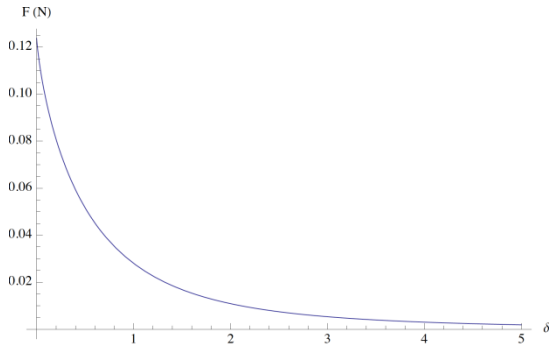

(a). $F_{3,2}(\delta)$

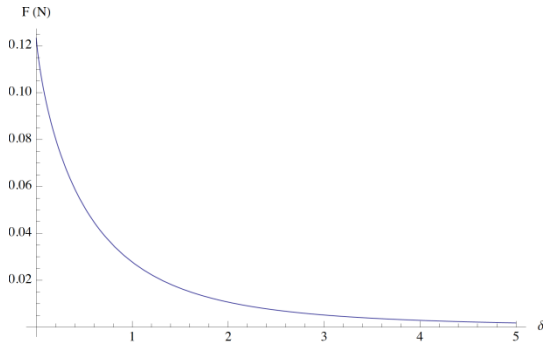

(b). $F_{2,2}(\delta)$

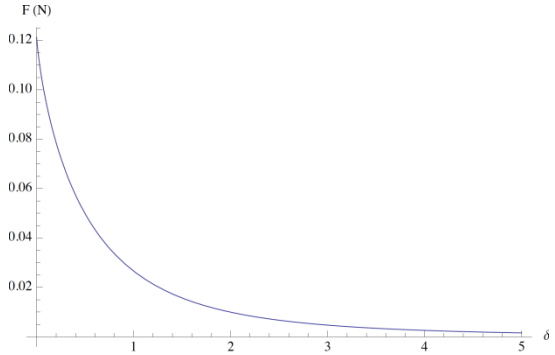

(c). $F_{1,4}(\delta)$

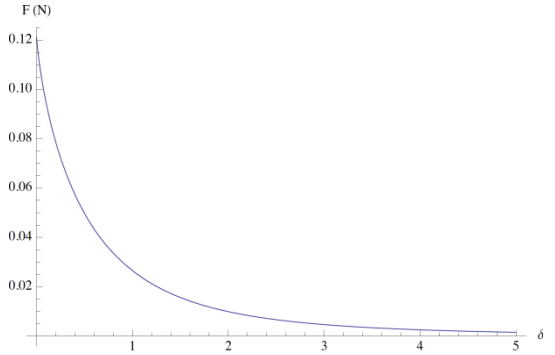

(d). $F_{1,3}(\delta)$

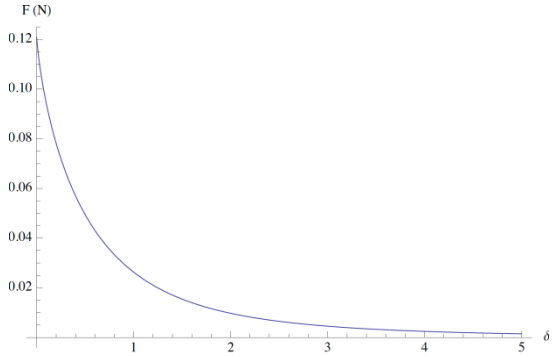

(e). $F_{1,2}(\delta)$

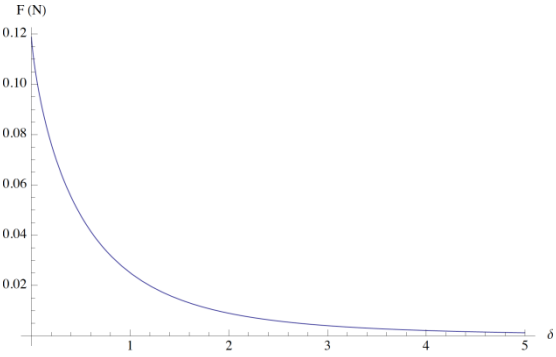

(f). $F_{1,1}(\delta)$

Figure 3.7 Force of separation for (a) three magnets from two magnets (b) two magnets from two magnets (c) one magnet from four magnets (d) one magnet from three magnets (e) one magnet from two magnets, and (f) one magnet from another magnet

Table 3.2. Force of separation for various magnet sequences

i,j (i magnets being separated from j magnets in a n magnet configuration)	$F_{i,j}$ (Force to separate i magnets from j magnets in Newtons)
3,2 (n=5)	0.123697
1,4 (n=5)	0.121257
2,2 (n=4)	0.123259
1,3 (n=4)	0.121157
1,2 (n=3)	0.120819
1,1 (n=2)	0.118717

Therefore, it can be concluded that the failure follows the sequence (1,4); (1,3); (1,2); (1,1), i.e. magnet separation always occurs at either ends of the magnet-string configuration.

3.2.2 Response Modeling for the Healing Configuration

Based on the configuration in Figure 3.5, the loading of the secondary member follows the sequential, progressive failure of a primary load path consisting of n magnets. Upon loading of the configuration, the primary load path consists entirely of magnets carrying the load. However, despite all the magnets being identical, the theoretical failure load will be affected by the force of attraction between adjacent magnets, as well as the force of attraction between the magnets further away. The failure loads cause the configuration to fail sequentially, one magnet link at a time, instead of simultaneously. Upon separation of the magnets, the system partially unloads, similar to the original tailored composite configuration, thereby causing a beneficial strain energy loss in the system. However, with every increasing subsequent separation, the string of secondary load path starts loading before the system completely unloads. The unloading-loading behavioral sequence of the system will continue until the system is loaded to its maximum, such that once all the primary segments have failed, the secondary load path eventually fails under the load. The characteristic response of the configuration can be modeled by developing a mathematical model consisting of a system of equations that define the states of equilibrium for the magnet-string configuration under loading conditions until the secondary load path eventually fails.

Beginning with the initial magnet separation, the force of attraction between the magnets and the extension forces in the string are determined for before and after every subsequent magnet separation until the string eventually fails. The basic configuration parameters taken into account for modeling the response of configuration are introduced in Table 3.3 below.

Table 3.3. Basic configuration parameters

Parameter	Description
l	Length of primary segment i.e. magnet (m)
d	Diameter of primary segment i.e. magnet (m)
l_s	Length of unloaded string
δ	Normalized End displacement in the string on loading
F	Applied load (N)
k	Stiffness (N/m)
ε_f	Ultimate failure strain
n	Number of links

The distance between the two magnet centers can be recast in terms of the parameters in Table 3.3 as,

$$\varsigma = (\frac{l_1}{2} + \frac{l_2}{2} + x)\frac{1}{R}\hat{E}\hat{E}\frac{l_1}{2R} + \frac{l_2}{2R} + \delta \tag{3.5}$$

where, x is the separation distance between the ends of the magnets.

In order to analyze the forces acting on the system when it is under loading, a part of the system is represented in Figure 3.8. The dotted area represents the section considered for studying the forces acting upon the system. This area also represents a functional link in the system. A free-body diagram of the functional link of the n-magnet system has been illustrated in Figure 3.9 below to analyze the forces acting on the link when the system is loaded. The free body diagram illustrates that the forces acting on the link are in equilibrium with the total applied force acting on the system.

The area under the dotted circle that has been considered for the free body diagram consists of a part of the system that comprises a magnet and loaded strings that are attached to

the magnet along its length. The free body diagram illustrates that the forces acting on the link are the force between the magnets F_1, and the force in each string $F_s/2$. Therefore, the total force in the strings F_s is the sum of the forces in the individual strings. The total displacement in the system being δ, the force in the string F_s is equal to k (δ). The total applied force F acting on the system is equal to the sum of all the forces acting on the link, namely the force between the magnets and the force in the strings.

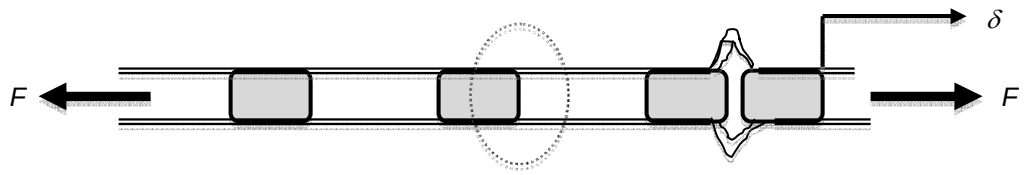

Figure 3.8 Magnet-string configuration for n-magnets

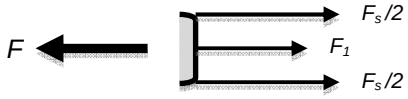

Figure 3.9 Free body diagram of a functional link of the magnet-string configuration

The mathematical model utilizes this equilibrium to define the equations of force and displacement for the system.

When a force is applied on a system consisting of n magnets, it starts loading, and continues to load until the first separation occurs at either end of the configuration. The force of separation between the magnets is denoted as F_1, where F_1 is a function of the number of magnets n, the distance between the ends of the magnets δ, and the computational stage i, which represents every successive magnet separation. For a system consisting of n magnets, the number of magnet separations is equal to n-1.

After every magnet separation, the separated magnets continue to be pulled apart until the strings become straight. The unloaded strings i.e. the straightened strings between the separated magnets start loading as the applied force continues to stretch the configuration. This

load in the system is denoted as F_2. The string continues to elongate until the load in the system is sufficient to bring about a subsequent magnet separation.

Eq. 3.6 gives the force of separation between the magnets, F_1, after the system is loaded. Eq. 3.7 represents the load in the system when the strings are loaded F_2, at every computational stage *i*.

$$F_1(n,i) = F_{1,n-i}(\frac{\delta}{i}), \quad \delta_1(i) < \delta < \delta_2(i) \tag{3.6}$$

$$F_2(n,i) = F_{1,n-i}(\frac{\delta}{i}) + k(\frac{\delta - il_s}{i}), \quad \delta_2(i) < \delta < \delta_3(i) \tag{3.7}$$

The displacement in the system is defined by equating the load in the string to the force required for every magnet separation.

δ_1 in Eq. 3.8 indicates the first magnet separation in the system, hence 0, whereas, δ_1 and δ_3 in Eqs. 3.9 and 3.11 respectively correspond to the displacement in the system (taut length of the string between separated previously magnets) representing every magnet separation. Eq. 3.10 denotes the unloaded length of the string, δ_2 prior to every magnet separation. Extension beyond the unloaded length indicates loading in the string as a result of the stretching force being applied on the configuration, which eventually results in magnet separations.

The displacements of the configuration under the event of loading, during every computational stage i are therefore determined by using the following equations,

$$\delta_1(i) = 0, \quad i = 1 \tag{3.8}$$

$$\delta_1(i) \Leftrightarrow F_{1,n-i} = F_2(i), \quad i = \{2,3,....,n-2\} \tag{3.9}$$

$$\delta_2(i) = il_s, \quad i = \{1,2,3....,n-1\} \tag{3.10}$$

$$\delta_3(i) \Leftrightarrow F_{1,n-i-1} = F_2(n,i) \tag{3.11}$$

For a *n*-magnet system, *n*-1 magnet separations is representative of the complete failure of the primary segment. However, despite this failure, the configuration continues to carry load through the string, which continues to load until it ultimately fails completely. The displacement in the system representing the complete failure of the primary segment is given by $\delta_{(n\text{-}2)th}$. The failure criteria for the string, is as given in Eq. 3.12,

$$\delta_f = \delta_{(n-2)^{th}} + l_s(\varepsilon_f + 1)(n-1) \tag{3.12}$$

l_s (ε_f+1)(*n*-1) represents the total extension in the string, leading to failure due to the applied load, even beyond the final magnet separation.

The model is then implemented as a Mathematica notebook, and a response for the model can therefore be developed for n magnets. Figure 3.10, illustrates the response of the magnet-string configuration under loading for multiple magnet configuration.

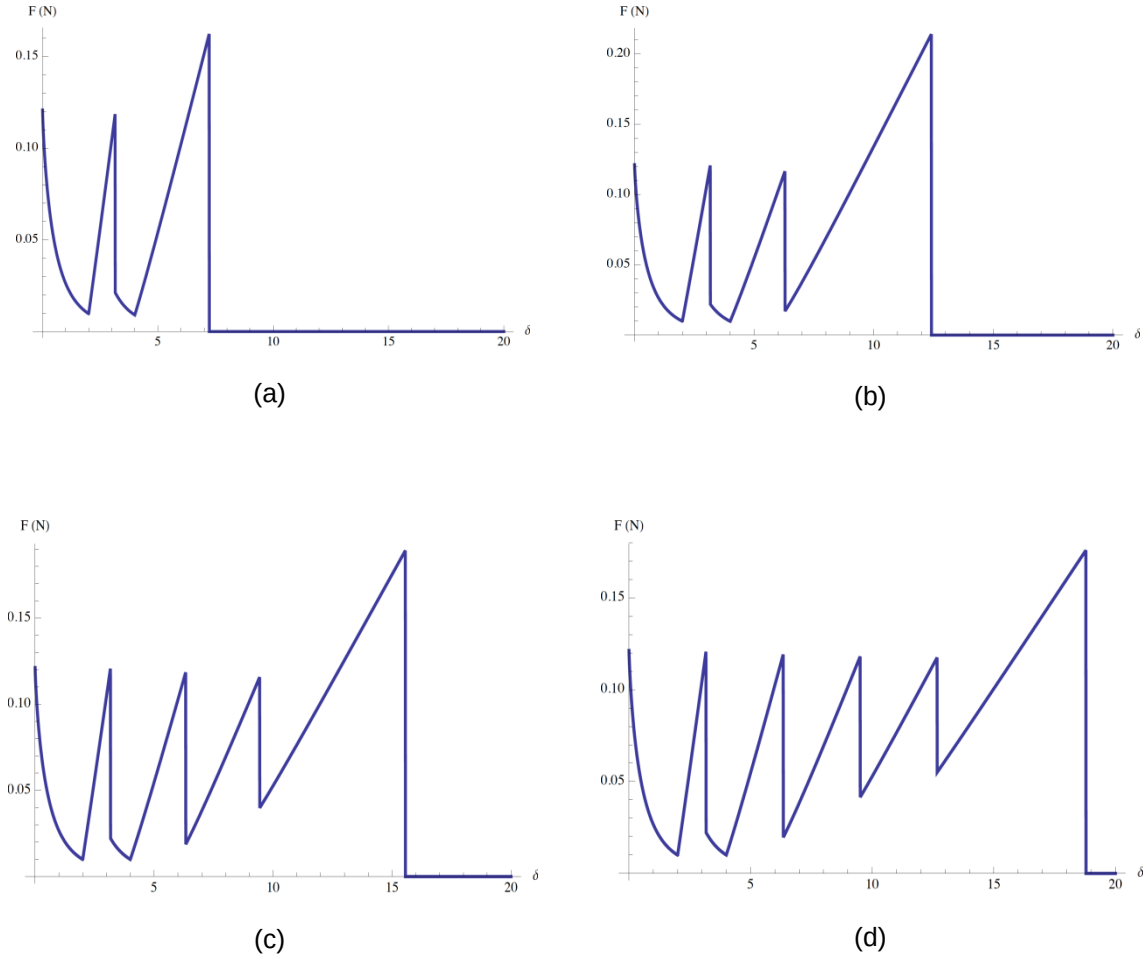

Figure 3.10 Load (F)-displacement (δ) curve for (a) 3-magnet configuration, (b) 4-magnet configuration, (c) 5-magnet configuration, and (d) 6-magnet configuration

CHAPTER 4

RESULTS AND DISCUSSION

Progressive failure (and reconstitution) of n magnets, followed by the failure of a single secondary segment characterizes the failure of the magnet-string configuration. The force of attraction between the magnets governs the failure sequence such that a separation occurs at either end of the configuration. Prior to the failure of the secondary segment, there are *n*-1 stages of separation in response to the applied load. Every stage is in turn characterized by unloading of the system, followed by the loading of the secondary segments.

A tensile load applied to the ends of the magnet-string configuration transmits to the functional link of the configuration, which consists of the magnets, string and the connector segments. After the initial separation, the load in the system drops drastically. However, the system never completely unloads because there are always magnetic forces that keep the tether loaded. The string then starts to load under continued loading. This continues until the load in the string is sufficient to cause the next separation. This continues for every link until every magnet has separated. Then, only the string carries the load in the system after the complete failure of the primary segment. This continues until the string ultimately fails.

For the secondary segments arranged in series the compliance of the system increases after every subsequent separation. However, the compliance of the segments remains unchanged since the strings never change their properties or dimensions. It is essential that the failure load for the string is higher than that for any magnet separation. Otherwise, the tether would fail if the string were to fail prior to the failure of the primary segment, thereby rendering the healing concept redundant. Hence, the material properties are selected such that all the

magnets separate prior to the loading and the eventual failure of the string. It must be noted that the when the configuration is loaded, under no circumstances must the magnets experience mechanical failure due to de-cohesion. It is therefore important for the magnets to be made out of a very strong material. The Neodymium magnets used to model this configuration have adequate mechanical strength to ensure that this failure does not occur, and the only failures occurring in the system are the separation of magnets and the ultimate failure of the string.

As shown in Figure 4.1 below, it is observed that for every subsequent separation after the first two separations, the system begins loading immediately after the magnet separation, rather than continuing to unload after the magnet separation. An explanation for this is that the unloaded length of the string during these separations gets added to the loaded strings between the previously separated magnets. This causes the strings to relax, but not enough to allow the system to completely unload. Therefore, the system only partially unloads before it starts loading again, thereby leading to the next separation.

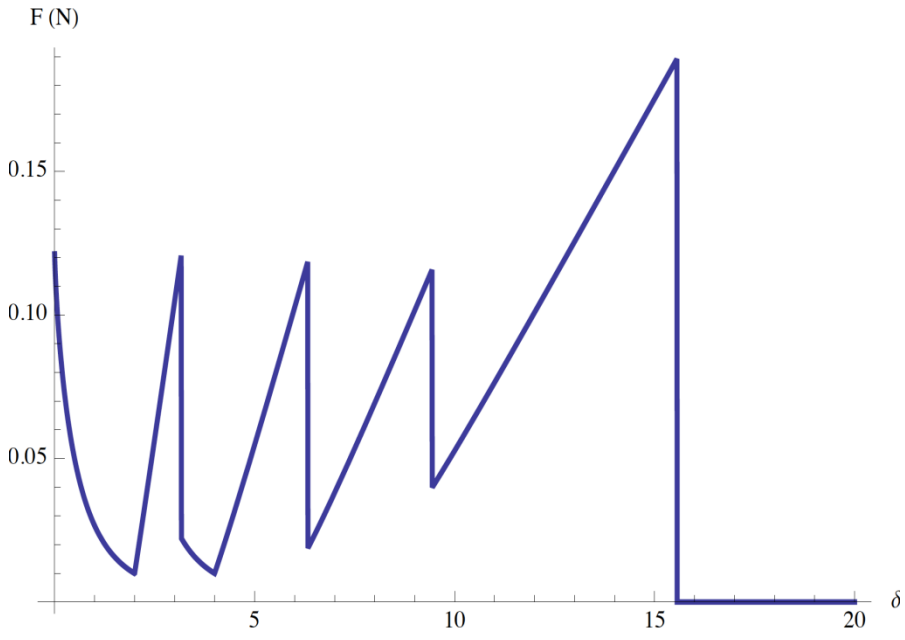

Figure 4.1 Load-displacement curve for a 5 magnet system

Consider a three-magnet system, like the one shown in Figure 3.8. For the case where the distance between three magnets is less than the length of two unloaded strings, there are three equilibrium points - two stable and one unstable, as illustrated in Figure 4.2. It is extremely difficult to model the dynamic system with damping and would require more material properties, so an assumption is made as to its final resting place. For the case where the distance between three magnets is greater than or equal to the length of the two unloaded strings between them, there is only one equilibrium point. This point represents the state of unstable equilibrium, and is an important consideration taken into account to configure the system. When a magnet separation occurs as a result of the applied load on the system, the force acting on the separated magnet imparts some acceleration to it, which enables the magnet to travel in the direction of a previously separated magnet. The momentum of the magnet continues to move forward until the forces in the string between the magnets and the forces between the magnets are balanced. This continues until the magnet velocity reduces to zero, which would mean that the kinetic energy in the magnet gets converted into strain energy of the string. From the point of magnet separation to the point where the separated magnet no more possesses a velocity, the string between the separated magnets is either flexing or straight, just prior to loading. However, when the string between the separated magnets possesses sufficient strain energy, it pulls the magnet back towards the other un-separated magnets. This would continue until the magnet possesses no more velocity to move forward, and would therefore be pulled back again. It is important to note that the velocity of the magnets is always non-zero in the state of equilibrium. It is only for the expectation of damping that the system would ever come to stop.

Equilibrium would imply that there exists a greater force of attraction between the magnets that are relatively closer to each other. While this represents stable equilibrium, a larger force is required to maintain this stability. Hence the system is modeled by assuming an unstable equilibrium, as shown in Figure 4.2 (c).

This also explains the discontinuity in the load-displacement plots during the separation that follows the initial separation in the system. As illustrated in Figures 4.2 (a) and 4.2 (b) respectively, in either state of stable equilibrium, the force between the magnets closer to each other is greater than the magnets that are farther away. This implies that there exist multiple positions of equilibrium while the dynamic process is occurring, which, although can be explained theoretically, is not captured by this particular model. The prediction of the final resting place of the magnets will depend on the configuration, and other properties not accounted for, such as damping. This region could be referred to as the meta-stable region. However, an investigation into this feature is a subject for future study.

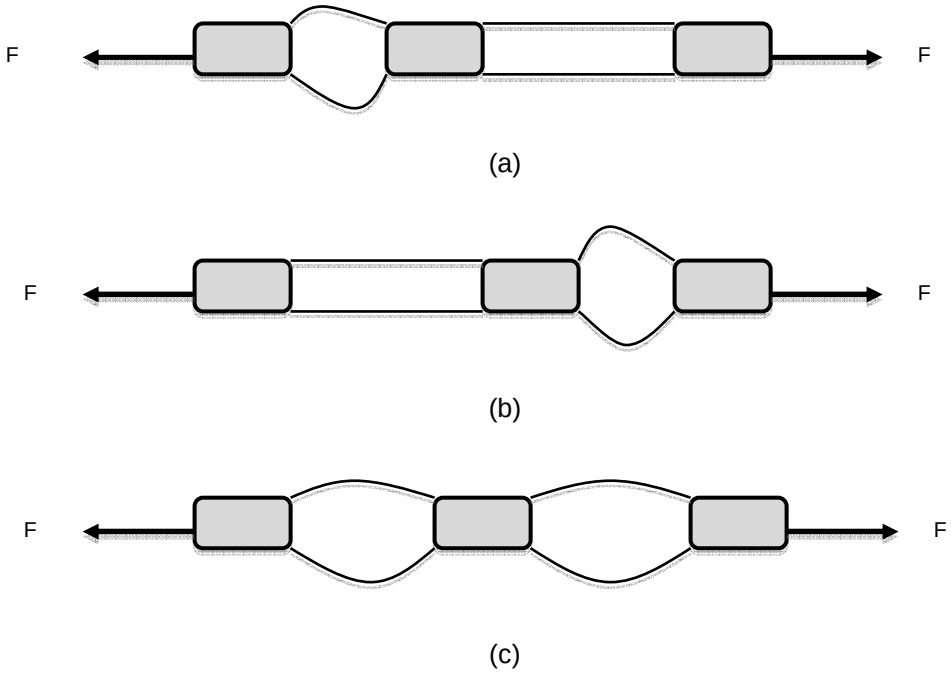

Figure 4.2 Types of equilibrium in the system (a) Stable equilibrium (b) Stable equilibrium, and (c) Unstable equilibrium

4.2 Interpreting the Results

The configuration parameters used to establish equilibrium in the configuration could be arbitrarily varied. Specific parameters are considered to study the magnet string configuration.

4.2.1 Varying the Aspect Ratio (l/d)

The aspect ratio of the primary segment i.e. the magnets has a considerable influence on the load-displacement profile of the configuration. The parameters for this exercise are provided in Table 4.1. A prominent change in the load-displacement profile is observed on changing the aspect ratios. The force required to separate one magnet from *n* magnets, where $2 \leq n \leq 20$, is determined by using Eq. 3.3. Using the parameters given in Table 4.1, when l>d, the normalized force required to separate 1 magnet from 19 magnets in a series of 20 magnets is considered to be 1. The force to separate 1 magnet from *n* magnets as *n* reduces from 19 to 2 is as follows-

{1, 0.999999, 0.999996, 0.999994, 0.999991, 0.999988, 0.999982, 0.999976, 0.999966, 0.999952, 0.999933, 0.999903, 0.999855, 0.999772, 0.999617, 0.999291, 0.998469, 0.995683, 0.97836} This indicates a very small yet steady decrease in the force of separation between the magnets.

When l<d, the magnets resemble a penny unlike cylinders when l>d. This affects the force of separation for 1 magnet from n magnets when n reduces from 19 to 2 as follows-

{1, 0.999848, 0.999661, 0.999426, 0.999131, 0.998751, 0.998256, 0.9976, 0.996712, 0.995482, 0.993731, 0.991162, 0.987251, 0.981039, 0.970658, 0.952243, 0.917156, 0.844183, 0.671712} There is a substantial decrease in the forces to separate the magnets as the number of stacked magnets decreases, with a significant drop in the force to separate 1 magnet from simply 1 or 2 magnets.

The change in the aspect ratios has a notable effect on the beneficial energy dissipated from the system. For a system of 10 magnets, the aspect ratio of magnets in Figure 4.3 (a) is l/d=2 (l>d), whereas the aspect ratio of the magnets in Figure 4.3 (b) is l/d=0.25 (l<d). The same

exercise is repeated for a system of 20 magnets, as shown in Figure 4.3 (a) and (b) respectively.

Table 4.1 Specific configuration parameters

Parameter	Description
l	0.25 cm; 0.03125 m
d	0.125 m
l_s	0.25 m (δ=2)
k	0.1 N/m
ε_f	0.02
n	10; 20

4.2.2 Varying Unloaded Length of String (l_s)

Figure 4.6 illustrates the load-displacement profile for a system of 10 magnets. On loading, a magnet at either end will separate from the rest of magnets at a force of approximately 0.124 N, as indicated by the arrow in Figure 4.6 (a). The system then unloads until the string becomes taut, whereupon the string loads until the second magnet separation occurs. After every subsequent separation, the system unloads, as evidenced by every peak in the figure below. This continues until the final separation, beyond which the applied load is carried completely by the string until the load in the string reaches the failure load of the string. The tether fails at a load of 0.285 N. A notable difference in the load-displacement profile is observed if the length of the unloaded string is varied while still maintaining the material properties. If the length of the unloaded string is increased while maintaining the other parameters, the area under the curve increases, as illustrated for a system of 10 magnets in Figure 4.6 (b). However, this increase in the area, which represents the energy dissipated from the system, is not necessarily beneficial. An increase in the length of the unloaded string would mean increase in the use of material. This implies that mass penalty would be incurred.

Similar observations are made when the same exercise is carried out for a system of 10 magnets and 20 magnets, as illustrated in Figures 4.6 and 4.7 respectively. The parameters considered for this exercise are as shown in Table 4.2 below.

Table 4.2 Specific configuration parameters (for varying l_s)

Parameter	Description
l	0.25 m
d	0.125 m
l_s	0.25 m; 0.625 m (δ=2; 5)
k	0.1 N/m
ε_f	0.02
n	5; 10; 20

On comparing Figure 4.5 (a) to Figures 4.6 (a) and 4.7 (a), it is observed that an increase in the beneficial energy dissipated from the system (work done) is achieved as the length of the primary load path increases. An increase in the length of the primary load path allows greater redistribution of load within the system. This means an increased toughness as the length of the primary load path increases.

However, it must be noted that these values reflect the response of the configuration with regards to the parameters selected for conducting this study. They do not represent an upper bound on the capabilities of the healing configuration.

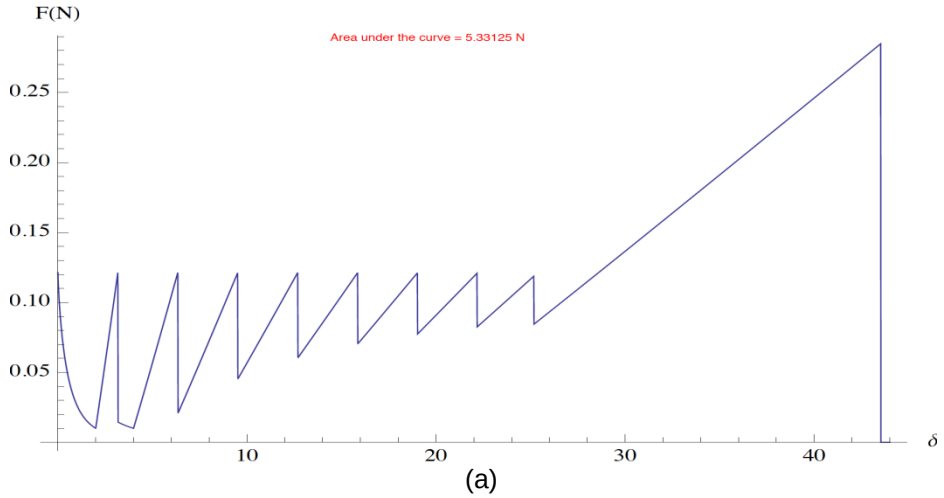

(a)

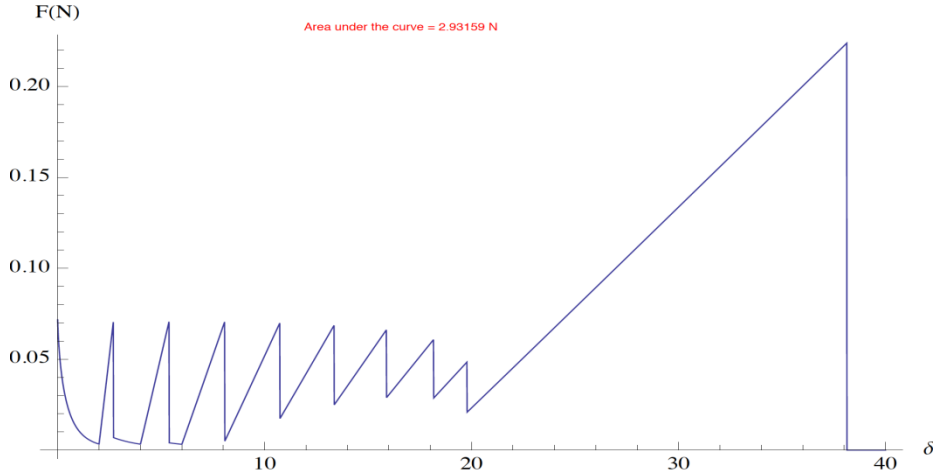

(b)

Figure 4.3 Load-displacement curve for 10 magnets when (a) l>d and (b) l<d

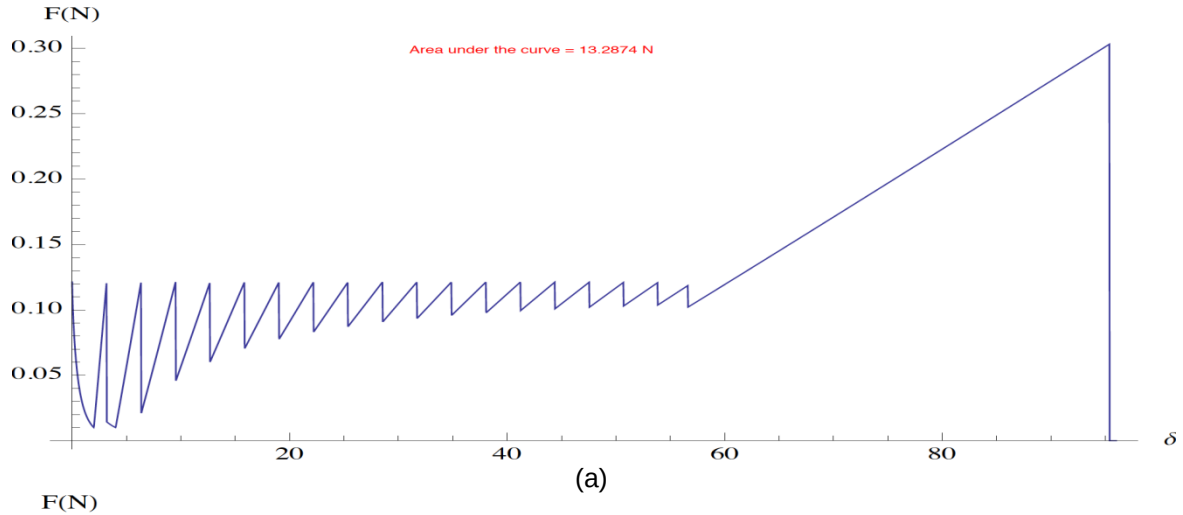

(a)

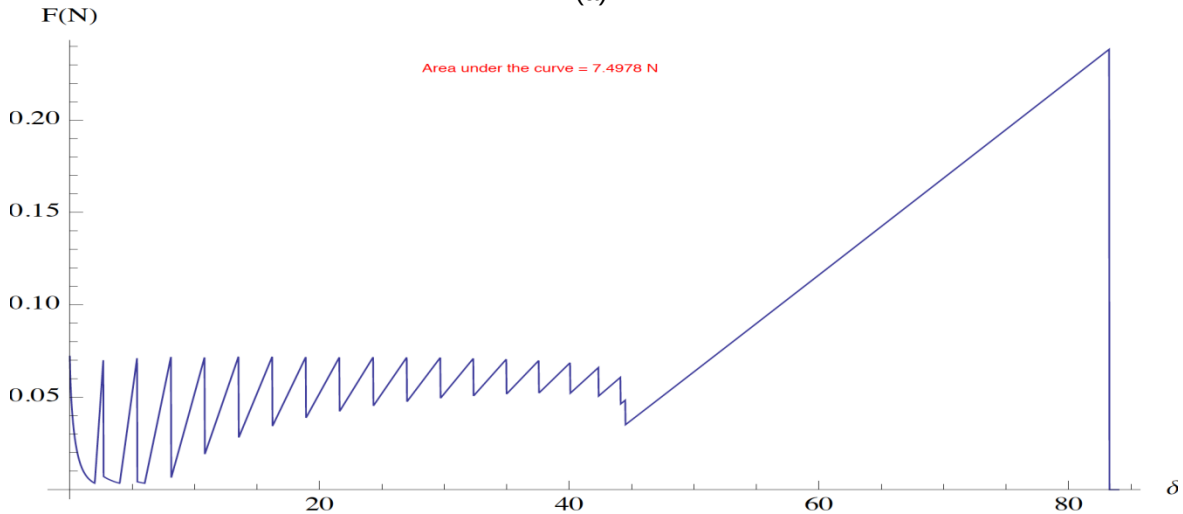

(b)

Figure 4.4 Load-displacement curve for 20 magnets when (a) l>d and (b) l<d

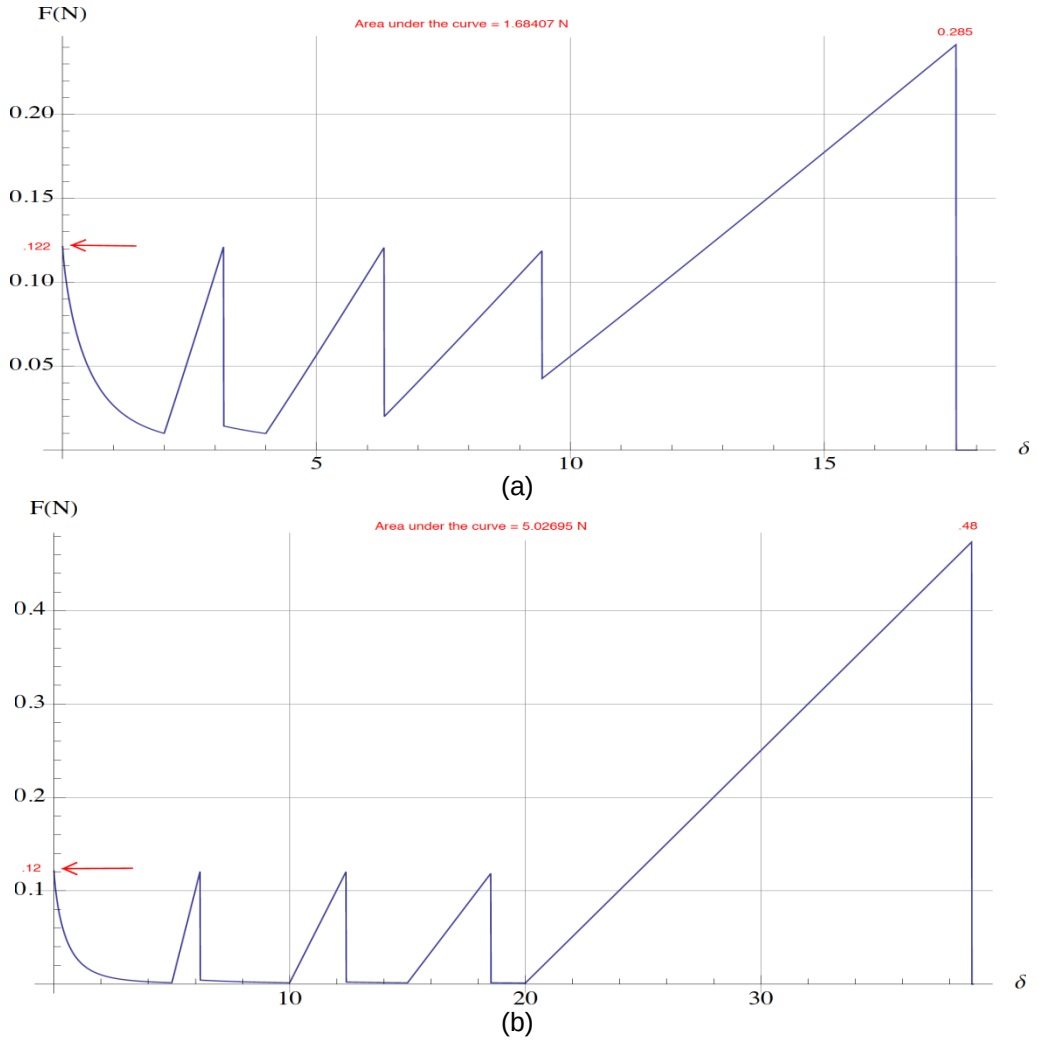

Figure 4.5 Load-displacement curve for (a) 5 magnets (l_s=2), and (b) 5 magnets (l_s=5)

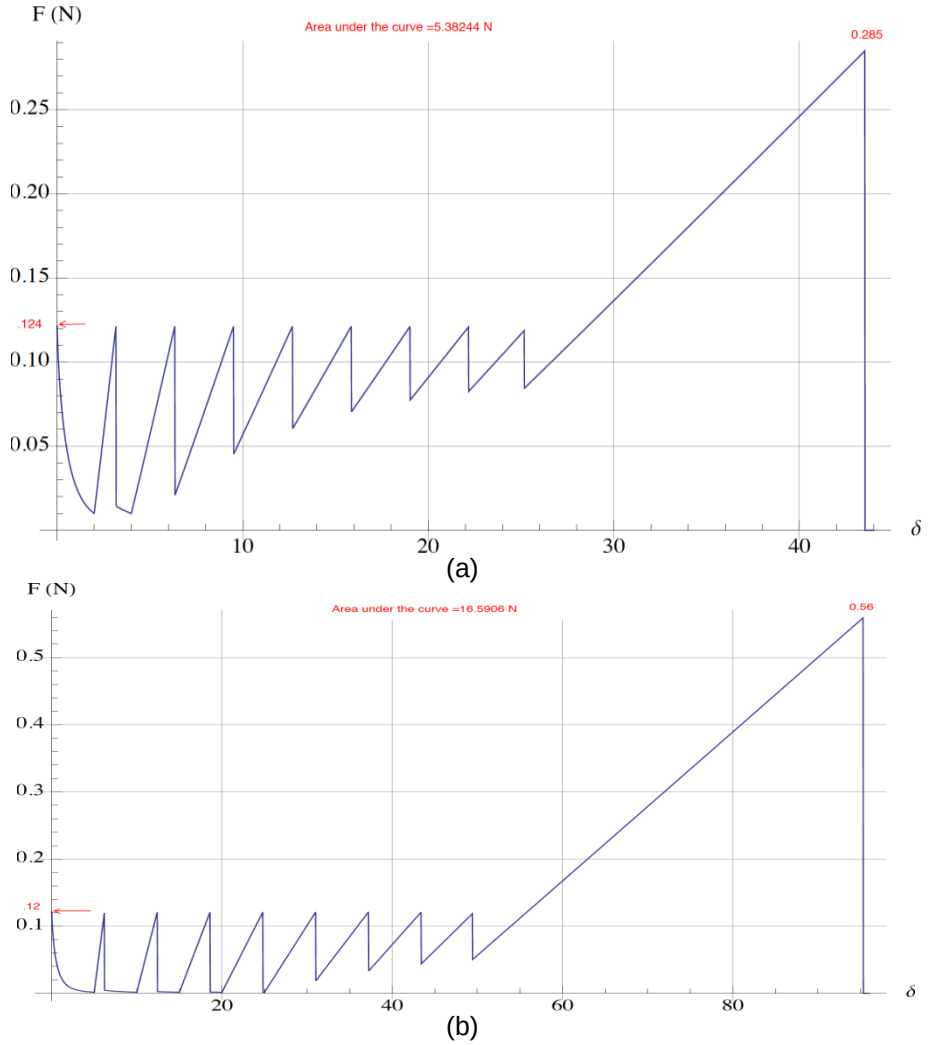

Figure 4.6 Load-displacement curve for (a) 10 magnets (l_s=2), and (b) 10 magnets (l_s=5)

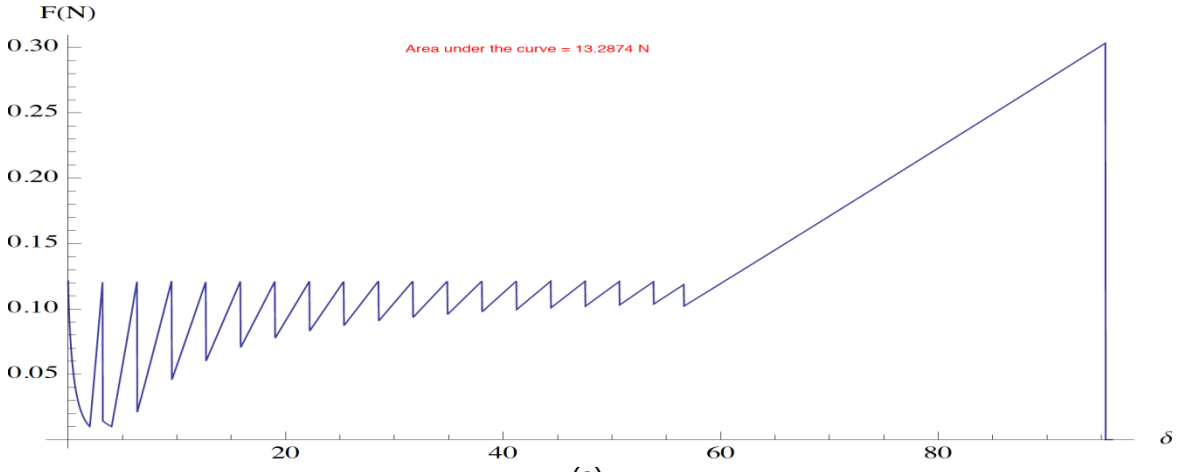

(a)

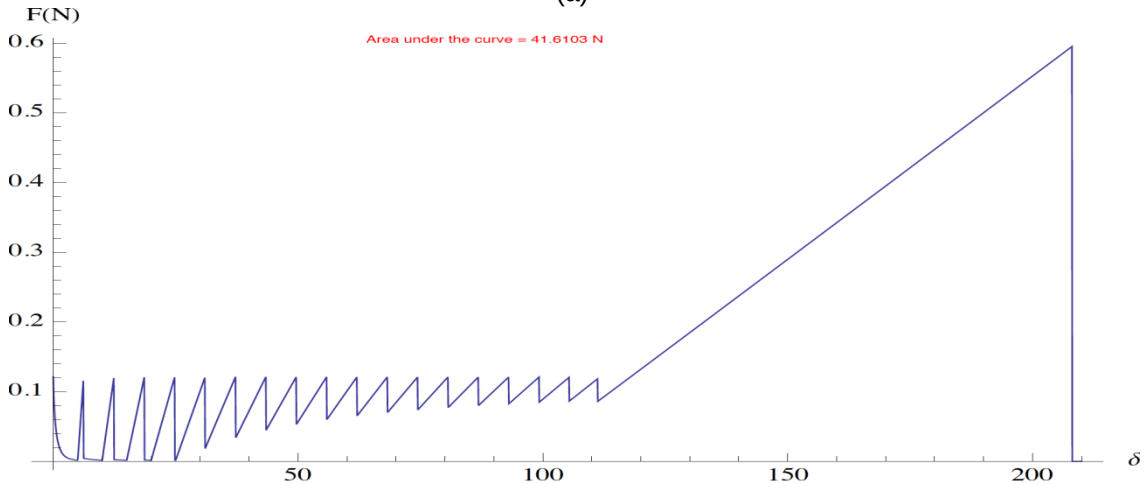

(b)

Figure 4.7 Load-displacement curve for (a) 20 magnets (l_s=2), and (b) 20 magnets (l_s=5)

CHAPTER 5

CONCLUSIONS AND RECOMMENDATIONS

5.1 Conclusions

A solution to the irreversibility of the original tailoring concept has been proposed and investigated in the form of an extension of the original concept. Magnets are used as primary segments and a polymer string is used as a secondary segment as opposed to the high performance composite fibers used in the original tailoring concept. The force of attraction between the magnets gives the configuration a healing characteristic. The response of the configuration is modeled such that it captures the essence of the original concept. Varying the governing configuration parameters can vary the response of the configuration. It can also be demonstrated that the configuration achieves a gain in the energy dissipation.

5.2 Recommendations for Future Work

The healing model developed in this research has been investigated analytically. However, an experimental validation is necessary to validate the analytical model.

Conducting a parametric study on the magnets-string configuration would be helpful in identifying the upper bounds regarding the performance of the concept. This can be achieved by converting the dimensional configuration parameters that govern the response of the system to non-dimensional parameters through appropriate algebraic manipulations. The non-dimensional parameters would be independent of a material system and thus useful in providing an unbiased comparison between the behavior of various configurations or material choices.The parametric study is currently in progress and Table 5.1 provides the reduced parameters being used in the study

Table 5.1 Reduced configuration parameters

Parameter	Description	Reduced Parameter	Definition
E	Modulus of elasticity	E'	K_d/E
K_d	Magnetostatic energy constant	(none)	-
l	Length of primary segment i.e. magnet	(none)	-
d	Diameter of primary segment i.e. magnet	(none)	-
l_s	Length of unloaded string	l'	l_s/l
δ	Displacement in the string on loading	δ'	δ/l
F	Applied load	F'	F/(E.A)
A	Cross-sectional area of the string	A'	A/l^2
τ	Aspect ratio of the magnet	τ	l/d
ε_f	Ultimate failure strain	ε_f	No change
n	Number of links	n	No change

An additional point of interest in the response obtained for the various magnet–string configurations is that, upon every subsequent separation of the magnets, the system unloads before it begins loading again. The discontinuity in the load carried by the system illustrates this behavior. At this point, the system is characterized by a meta-stable configuration.

APPENDIX A

A GENERAL FUNCTION TO DETERMINE THE LOAD – DISPLACEMENT PROFILE FOR n MAGNETS

```
ClearAll["Global`*"]

d = 0.125;
l = 0.25;

k = 0.1;
ϵf = 0.02;

ls = 2;

n = 5;

F11 = NIntegrate[((BesselJ[1, q]^2) / q) *
    Sinh[q l / d] * Sinh[q l / d] * Exp[-(l / d + l / d) q], {q, 0, ∞}];

IGv = Table[i F11 / k + i ls, {i, n - 2}];

F22 = Table[NIntegrate[((BesselJ[1, q]^2) / q) * Sinh[q l / d] *
     Sinh[q (n - i - 1) l / d] * Exp[-(l / d + (n - i - 1) l / d) q], {q, 0, ∞}], {i, n - 2}];

F[δ_?NumericQ] :=
  (k / i) (δ - i ls) + NIntegrate[((BesselJ[1, q]^2) / q) * Sinh[q l / d] *
     Sinh[q (n - i) l / d] * Exp[-(l / d + (n - i) l / d + δ / i) q], {q, 0, ∞}];

db = Table[FindRoot[F[δ] == F22[[i]], {δ, IGv[[i]]}], {i, n - 2}];

Piecewise[Flatten[
  Table[{{Integrate[((BesselJ[1, q]^2) / q) * Sinh[q l / d] * Sinh[q (n - i) l / d] *
       Exp[-(l / d + (n - i) l / d + x / i) q], {q, 0, ∞}],
     If[i == 1, 0, δ /. db[[i - 1]]] < x ≤ i ls},

    {Integrate[((BesselJ[1, q]^2) / q) * Sinh[q l / d] *
        Sinh[q (n - i) l / d] * Exp[-(l / d + (n - i) l / d + x / i) q], {q, 0, ∞}] +
      ((k / i) (x - i ls)), i ls < x < If[1 ≤ i ≤ n - 2, δ /. db[[i]],
       N[δ /. db[[i - 1]]] + ls (ϵf + 1) (n - 1)]}}, {i, n - 1}], 1]]
```

```
ConditionalExpression[
  1/8 (1. + 0.31831 x^2 EllipticE[-4./x^2] +
      (-1.27324 - 0.31831 x^2) EllipticK[-4./x^2] - 1/π
      (π + (4. + 1. x)^2 EllipticE[-4./(4. + 1. x)^2] +
        (-20. + (-8. - 1. x) x) EllipticK[-4./(4. + 1. x)^2]) -
      1/π (π + (16. + 1. x)^2 EllipticE[-4./(16. + 1. x)^2] +
        (-260. + (-32. - 1. x) x) EllipticK[-4./(16. + 1. x)^2]) +
      1/π (π + (20. + 1. x)^2 EllipticE[-4./(20. + 1. x)^2] +
        (-404. + (-40. - 1. x) x) EllipticK[-4./(20. + 1. x)^2]))      0 < x ≤ 2
  0.1 (-2 + x) + 1/8 (1. + 0.31831 x^2 EllipticE[-4./x^2] + (-1.27324 - 0.31831 x^2)      2 < x < 3.16944
      EllipticK[-4./x^2] - 1/π (π + (4. + 1. x)^2 EllipticE[-4./(4. + 1. x)^2] +
        (-20. + (-8. - 1. x) x) EllipticK[-4./(4. + 1. x)^2]) -
      1/π (π + (16. + 1. x)^2 EllipticE[-4./(16. + 1. x)^2] +
        (-260. + (-32. - 1. x) x) EllipticK[-4./(16. + 1. x)^2]) +
      1/π (π + (20. + 1. x)^2 EllipticE[-4./(20. + 1. x)^2] +
        (-404. + (-40. - 1. x) x) EllipticK[-4./(20. + 1. x)^2]))
  1/8 (1. + 0.0795775 x^2 EllipticE[-16./x^2] -      3.16944 < x ≤ 4
      1/π (π + (4. + 0.5 x)^2 EllipticE[-4./(4. + 0.5 x)^2] +
        (-20. + (-4. - 0.25 x) x) EllipticK[-4./(4. + 0.5 x)^2]) -
      1/π (π + (12. + 0.5 x)^2 EllipticE[-4./(12. + 0.5 x)^2] +
        (-148. + (-12. - 0.25 x) x) EllipticK[-4./(12. + 0.5 x)^2]) +
      1/π (π + (16. + 0.5 x)^2 EllipticE[-4./(16. + 0.5 x)^2] +
        (-260. + (-16. - 0.25 x) x) EllipticK[-4./(16. + 0.5 x)^2]) +
      (-1.27324 - 0.0795775 x^2) EllipticK[-16./x^2])
  0.05 (-4 + x) + 1/8 (1. + 0.0795775 x^2 EllipticE[-16./x^2] -      4 < x < 6.3329      , x ≥ 17.5984 || x = 3.16944 || x ≤ 0 || Re[x] > 0
      1/π (π + (4. + 0.5 x)^2 EllipticE[-4./(4. + 0.5 x)^2] +
        (-20. + (-4. - 0.25 x) x) EllipticK[-4./(4. + 0.5 x)^2]) -
      1/π (π + (12. + 0.5 x)^2 EllipticE[-4./(12. + 0.5 x)^2] +
        (-148. + (-12. - 0.25 x) x) EllipticK[-4./(12. + 0.5 x)^2]) +
      1/π (π + (16. + 0.5 x)^2 EllipticE[-4./(16. + 0.5 x)^2] +
        (-260. + (-16. - 0.25 x) x) EllipticK[-4./(16. + 0.5 x)^2]) +
      (-1.27324 - 0.0795775 x^2) EllipticK[-16./x^2])
  0.0333333 (-6 + x) + 1/8 (1. + 0.0353678 x^2 EllipticE[-36./x^2] + 1/π (-3.14159 +      6 < x < 9.4384
        (-16. + (-2.66667 - 0.111111 x) x) EllipticE[-4./(4. + 0.333333 x)^2] +
        (20. + (2.66667 + 0.111111 x) x) EllipticK[-4./(4. + 0.333333 x)^2]) +
      1/π (-3.14159 + (-64. + (-5.33333 - 0.111111 x) x)
        EllipticE[-4./(8. + 0.333333 x)^2] +
        (68. + (5.33333 + 0.111111 x) x) EllipticK[-4./(8. + 0.333333 x)^2]) +
      1/π (π + (12. + 0.333333 x)^2 EllipticE[-4./(12. + 0.333333 x)^2] +
        (-148. + (-8. - 0.111111 x) x) EllipticK[-4./(12. + 0.333333 x)^2]) +
      (-1.27324 - 0.0353678 x^2) EllipticK[-36./x^2])
  0.025 (-8 + x) + 1/8 (1. + 0.0198944 x^2 EllipticE[-64./x^2] -      8 < x < 17.5984
      1/π 2 (π + (4. + 0.25 x)^2 EllipticE[-4./(4. + 0.25 x)^2] +
        (-20. + (-2. - 0.0625 x) x) EllipticK[-4./(4. + 0.25 x)^2]) +
      1/π (π + (8. + 0.25 x)^2 EllipticE[-4./(8. + 0.25 x)^2] +
        (-68. + (-4. - 0.0625 x) x) EllipticK[-4./(8. + 0.25 x)^2]) +
      (-1.27324 - 0.0198944 x^2) EllipticK[-64./x^2])
  0                      True
]
```

```
Plot[%, {x, 0, 18}, AxesLabel → {"δ", "F(N)"}, GridLines → Automatic]
(*Plot load vs. displacement*)
```

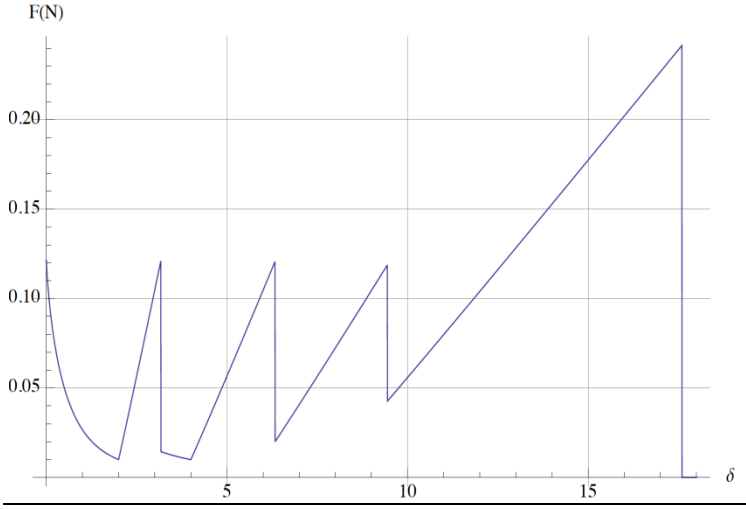


```
NIntegrate[%%, {x, 0, 18}] (*Area under the curve*)
```

```
1.68407
```

REFERENCES

[1] S. van der Zwaag, “An Introduction to Material Design Principles: Damage Prevention versus Damage Management”, *Self-Healing Materials*, S. van der Zwaag, Ed. Dordrecht, The Netherlands: Springer, 2007, pp 1-17

[2] www.tethers.com

[3] Hoyt, R.P., Forward, R.L., “Failsafe Multistrand Tether SEDS Technology”. *4th International Conference on Tethers in Space*, Washington, DC April 1995.

[4] Dancila, D. S., Armanios, E. A., “Energy Dissipating Composite Members with Progressive Failure: Concept Development and Analytical Modeling”. *AIAA Journal*, Vol 40. No. 10, 2002, pp 2096-2104

[5] Kessler, M.R., “Self-Healing: a new paradigm in materials design”. *Proc. IMechE Vol. 221 Part G: J. Aerospace Engineering (G4) (2007)*, pp 479-495

[6] Brown, E.N., Sottos, N.R., White, S.R. (2002), “Fracture testing of a self-healing polymer composite”. *Exp Mech 42*, pp 372-379

[7] Jones, A.S., Rule, J.D., Moore, J.S., White S.R., Sottos N.R. (2006), “Catalyst morphology and dissolution kinetics of self-healing polymers”. *Chem Mater 18*, pp 1312-1317

[8] Mauldin, T.C., Rule, J.D., Sottos, N.R., White, S.R., Moore, J.S. (2007), “Self-healing kinetics and the stereoiomers of dicyclopentadiene”. *J.R. Soc. Interface, 2007, 4(13)*, pp 389-393

[9] Rule, J.D., Brown, E.N., Sottos, N.R., White, S.R., Moore, J.S., “Wax-protected catalyst microspheres for efficient self-healing materials”. *Ad. Mater, 2005, 17*, pp 205-208

[10] S.R. White, N.R. Sottos, P.H. Geubelle, J.S. Moore, M.R. Kessler, S.R. Sriram, E.N. Brown and S. Viswanathan, “Autonomic healing of polymer composites”. *Nature* **409** (2001), pp. 794–797

[11] Stinson, S.C., (2000), “Chiral drugs”. *Chem Eng News* 78, pp 55-78

[12] Toohey, K. S.,White, S. R., and Sottos, N. R., **“**Self-healing polymer coatings”. *In Proceedings of the 2005 SEM Annual Conference and Exposition on Experimental and AppliedMechanics*, 2005, pp. 241–244

[13] Dry, C.**, “**Procedures developed for self-repair of polymer matrix composite materials”. *Compos. Struct.*, 1996, 35, pp 263–269

[14] Dry, C. M.**,** and Sottos, N. R, **“**Passive smart selfrepair in polymer matrix composite materials”. In *Smart structures and materials 1995: smart materials*, 3rd edition, (Ed. K. Varadian), *Proc. SPIE*, 1993, 1916, pp 438–444

[15] Hucker, M., Bond, I., Foreman, A.**,** and Hudd, J**. “**Optimisation of hollow glass fibres and their composites”. *Adv. Compos. Lett.*, 1999, 8(4), pp 181–189

[16] Trask, R. S. and Bond, I. P., **“**Biomimetic selfhealing of advanced composite structures using hollow glass fibres”. *Smart Mater. Struct.*, 2006, 15, pp 704–710

[17] Pang, J. W. C. and Bond, I. P., **“**Bleeding composites - damage detection and self-repair using a biomimetic approach”. *Compos. A, Appl. Sci. Manuf.*, 2005, 36, pp 183–188

[18] Pang, J. W. C. and Bond, I. P., **“**A hollow fibre reinforced polymer composite encompassing self-healing and enhanced damage visibility”. *Compos. Sci. Technol.*, 2005, 65, pp 1791–1799

[19] Kirkby, E.L., Rule, J.D., Michaud, V.J., Sottos, N.R., White, S.R., Manson, J.A.E., “Embedded shape-memory alloy wires for improved performance of self-healing polymers”. *Adv Funct Mater* 2008, 18, pp 2253–60

[20] Kessler, M.R., Sottos, N.R., White, S.R., “Self-healing structural composite materials”. *Composites* Part A 2003, 34, pp 743–53

[21] Rowan, S.J., Suwanmala, P., Sivakova, S., “Nucleobase-induced supramolecular polymerization in the solid state”. *J Polym Sci Part A Polym Chem* 2003,41, pp 3589–96

[22] Sivakova, S., Bohnsack, D.A., Mackay, M.E., Suwanmala, P., Rowan, S.J.,

"Utilization of a combination of weak hydrogen-bonding interactions and phase segregation to yield highly thermosensitive supramolecular polymers". *J Am Chem Soc* 2005,127, pp 18202–11

[23] Nair, K.P., Breedveld, V., Weck, M., "Complementary hydrogen-bonded thermoreversible polymer networks with tunable properties". *Macromolecules* 2008, 41, pp 3429–38

[24] de Lucca Freitas, L.L., Stadler, R. "Thermoplastic elastomers by hydrogen bonding. 3. Interrelations between molecular parameters and theological properties". *Macromolecules* 1987, 20, pp 2478–85

[25] Sijbesma, R.P., Beijer, F.H., Brunsveld, L., Folmer, B.J.B., Hirschberg, J.H.K.K, Lange, R.F.M., et al., "Reversible polymers formed from self-complementary monomers using quadruple hydrogen bonding". *Science* 1997, 278,pp 1601–4

[26] Rieth, L.R., Eaton, R.F., Coates, G.W., "Polymerization of ureidopyrimidinone-functionalized olefins by using late-transition metal ziegler-natta catalysts: synthesis of thermoplastic elastomeric polyolefins". *Angew Chem Int Ed* 2001,40, pp 2153–6

[27] Kersey, F.R., Loveless, D.M., Craig, S.L., "A hybrid polymer gel with controlled rates of cross-link rupture and self-repair". *J Roy Soc Interface* 2007, 4, pp 373–80

[28] Wool, R. P., and O'Conner, K. M., **"**A theory of crack healing in polymers". *J. Appl. Phys.* 1981, 52(10), pp 5953–5963

[29] Sanada, K., Yasuda, I., and Shindo, Y., **"**Transverse tensile strength of unidirectional fibre-reinforced polymers and self-healing of interfacial debonding". *Plast.,Rubber Compos.*, 2006, 35, pp 67–72

[30] Brown,E. N.,White, S. R., and Sottos, N. R**., "**Retardation and repair of fatigue cracks in a microcapsule toughened epoxy composite – Part I: manual infiltration". *Compos. Sci. Technol.*, 2005, 65, pp 2466–2473

[31] Brown,E. N.,White, S. R., and Sottos, N. R**., "**Retardation and repair of fatigue

cracks in a microcapsule toughened epoxy composite – Part II: In situ self-healing". *Compos. Sci. Technol.*, 2005, 65, pp 2474–2480

[32] Zako, M. and Takano, N.**, "**Intelligent material systems using epoxy particles to repair microcracks and delamination damage in GFRP". *J. Intel.Mater. Syst. Struct.*, 1999, 10, pp 836–841

[33] Ford, K. J. and Barbero, E. J., **"**Identification of continuum healing mechanics for polymer matrix composites". International SAMPE Symposium and Exhibition (Proceedings), 2005, vol. 50, pp 1739–1752

[34] Barbero, E. J., Greco, F., and Lonetti, P., **"**Continuum damage-healing mechanics with application to self-healing composites". *Int. J. Damage Mech.*, 2005, 14, pp 51–81

[35] Barbero, E. J., Ford, K. J., and Stiller, A., **"**Continuum damage healing mechanics for modeling of self-healing composites". International SAMPE Technical Conference, 2004, pp. 2681–2689

[36] Barbero, E. J. and Lonetti, P., **"**Application of continuum damage healing mechanics to self-healing composites". *Am. Soc.Mech. Eng., Aerosp.Div. (Publication)AD*, 2003, 68, pp 515–519

[37] Barbero, E. J. and Ford, K. J., **"**Identification of continuum healing mechanics for polymer matrix composites". *In Proceedings of McMat2005: 2005 Joint ASME/ASCE/SES Conference on Mechanics of Materials*, Baton Rouge, Louisiana, 1–3 June 2005, p 367

[38] Tian, W., Wang, X., Pan, Q., and Mao, Z., **"**Microcapsule used for self-healing polymer material". *Huagong Xuebao/J. Chem. Ind. Eng. (China)*, 2005, 56, pp 1138–1140

[39] Dancila, D. S., Armanios, E. A., "Energy Dissipating Composite Members with Progressive Failure: Impulsive Response and Experimental Verification", *AIAA Journal*, Vol 48. No. 4, 2010, pp. 728-737

[40] Haynes, Robert A., Dancila, D. S., Armanios, E. A., "Analytical Investigation of the Toughening Potential of a Failure tailoring Concept", *AIAA Journal*, Vol 48. No. 12, 2010, pp.

2945-2953

[41] Vokoun, D., Beleggia, M., Heller, L., Sittner, P., “Magnetostatic interactions and forces between cylindrical permanent magnets”, Journal of Magnetism and Magnetic Materials 321 2009, pp. 3758-3763.

BIOGRAPHICAL INFORMATION

Shailesh Jayant Divey was born on June 14, 1987 in Nagpur, India. He graduated with a Bachelor of Science degree in Metallurgical and Materials Engineering from the National Institute of Technology, Rourkela, India in June 2008. Subsequently he joined Continuous Caster at Essar Steel Ltd., India as a production engineer and held the position from June 2008 – June 2009, following which he joined the graduate program in the Department of Materials Science and Engineering at The University of Texas at Arlington in August 2009. He began working with Dr. D. Stefan Dancila in September 2009.